Research Square

Preprints are preliminary reports that have not undergone peer review.
They should not be considered conclusive, used to inform clinical practice,
or referenced by the media as validated information.

Valorization of pistachio shell waste into a biochar/Zeolite-13X composite for CO2 adsorption: Role of porous structure and surface chemistry

Mina Mollazadeh Azari
University of Tabriz
Ali Farzi
a-farzi@tabrizu.ac.ir

University of Tabriz

Research Article

Keywords: Biochar, Zeolite-13X, CO_2 adsorption, Pistachio shell waste, Composite adsorbent, Gas separation

Posted Date: November 16th, 2026

DOI: https://doi.org/10.21203/rs.3.rs-10618567/v1

License: This work is licensed under a Creative Commons Attribution 4.0 International License.
Read Full License

Additional Declarations: No competing interests reported.

Valorization of pistachio shell waste into a biochar/Zeolite-13X composite for CO_2 adsorption: Role of porous structure and surface chemistry

Mina Mollazadeh Azari[1], Ali Farzi[1*]

[1]Faculty of Chemical and Petroleum Engineering, University of Tabriz, Tabriz, Iran

Email: mina.mollazadeh@phd.tabrizu.ac.ir , a-farzi@tabrizu.ac.ir

Abstract

In the present investigation, a biochar-based adsorbent was prepared from pistachio shell waste-derived biochar (BPS). The obtained biochar was modified with Zeolite-13X particles to prepare a BPS/Zeolite-13X composite. The adsorbents were used to capture carbon dioxide from a gas stream. SEM-EDX, FTIR, BET, and XRD analyses were performed to characterize the obtained adsorbents. According to the results, the surface area of BPS and BPS/Zeolite- 13X was 184.74 and 357.05 m^2/g, respectively. The increase in surface area after the modification suggested that the surface properties of BPS were improved by adding Zeolite- 13X particles. Under the selected experimental conditions (80% CO_2 and 60 min), the experimental equilibrium CO_2 adsorption capacities (q_e) of BPS and the BPS/Zeolite-13X composite were 0.869 and 1.237 mmol g^{-1}, respectively. The highest adsorption capacity of the BPS/Zeolite-13X composite was obtained at a BPS/Zeolite-13X mass ratio of 70:30. The Sips isotherm predicted maximum adsorption capacities (q_m) of 1.04 and 1.54 mmol g^{-1} for BPS and BPS/Zeolite-13X, respectively. The isotherm and kinetic models demonstrated that the adsorption of CO_2 was best described by the Sips and pseudo-second-order models for BPS and BPS/Zeolite-13X adsorbents. The mechanism of CO_2 adsorption was clarified on the example of the BPS/Zeolite-13X composite, which revealed the presence of van der Waals forces, electrostatic attraction, and possible hydrogen bonding. Therefore, the fabricated adsorbent showed promising performance for CO_2 capture, demonstrating the potential of pistachio shell waste-derived materials.

Keywords: Biochar; Zeolite-13X; CO_2 adsorption; Pistachio shell waste; Composite adsorbent; Gas separation.

* **Corresponding Author: a-farzi@tabrizu.ac.ir**

1 Introduction

One of the main problems facing the world today is rising CO_2 levels in the atmosphere. Moreover, excessive global climate change is highly depended to carbon dioxide (CO_2) emissions that is a serious issue for environmental risks. The atmospheric CO_2 concentration has increased from 314 ppm in 1958 to 417 ppm in 2021. By 2100, it is expected to increase to 510 ppm in the next few decades. Consequently, it is important to control CO_2 emissions [1][2][3]. Three mainstream technologies for CO_2 capture have been developed: liquid absorption technology, membrane separation technology, and solid adsorption technology [4][5]. Solid adsorption technology, as an economical method, can be applied to solve this problem. The primary benefits of this approach, compared to other presented methods, are its cost-effectiveness, operational simplicity, and straightforward design. Besides, adsorption uses various low-priced and obtainable adsorbents such as biochar, zeolite, metal oxides, active carbons, and polymers, among others. Herein, biochar, Zeolite-13X, and their composite were selected for CO_2 adsorption from a gas stream [6].

Biochar, a highly porous, carbonaceous material, is obtained by anaerobic pyrolysis of biomass residues and is used as an adsorbent, catalyst, and soil conditioner. BC is effective in the adsorption process and has lower production costs than other carbon-rich materials [7][8][9]. Moreover, BC has attracted considerable attention owing to its high porosity, environmental compatibility, low cost, excellent stability, surface-enriched functional groups and aromatic surfaces, stable structure, easy synthesis methods, and favorable physical and chemical compatibility. However, the application of BC is limited owing to its inability to efficiently adsorb air pollutants, for instance, CO_2. Therefore, to enhance its performance, BC should be modified with special materials such as zeolite [10][11].

Zeolite is characterized by its porous crystalline structure that contains aluminosilicate minerals. It is formed by vertex-sharing of SiO_4 and AlO_4 tetrahedra with oxygen atoms to tetrahedral (TO_4) frameworks. The presence of aluminum atoms facilitates attraction of the oxygens and creates sites for cation exchange. These cations are instrumental in CO_2 capture, as they exhibit strong affinity toward CO_2 molecules within the zeolite matrix. Additionally, zeolite-based adsorbents exhibit great potential for CO_2 adsorption from industrial processes; this can be attributed to their advantage, such as suitable pore size, high surface area, and excellent thermal and chemical stability [12][13]. Among several types of zeolites, Zeolite-13X is one of the most effective adsorbents for CO_2 capture due to its high surface area, high cation-exchange capacity, and low Si/Al ratio. These characteristics have made it suitable for gas separation applications. Hydrothermal synthesis, organic template synthesis, microwave-assisted synthesis, and sol-gel synthesis are several methods for synthesizing zeolites. The hydrothermal method is the predominant technique for synthesizing zeolites, particularly when kaolin is used. Kaolin-based zeolites have a high CO_2 adsorption capacity due to the combination of microporous and mesoporous structures [14][15].

Combining biochar with zeolite can integrate the advantages of both materials, where biochar provides a high-surface-area carbon matrix, and zeolite contributes strong CO_2 adsorption sites with high affinity toward CO_2 molecules, leading to improved overall adsorption performance.

Accordingly, this study aims to synthesize pistachio shell waste-derived biochar (BPS) and subsequently modify it with Zeolite-13X to form a BPS/Zeolite-13X composite for efficient CO_2 capture. The effects of various factors, including contact time, CO_2 concentration, and

biochar-to-zeolite mass ratio, were investigated. Finally, adsorption isotherm and kinetic analyses were conducted to elucidate the adsorption behavior and mechanism of CO_2 uptake**.**

2 Materials and methods

2.1 Materials

Sodium hydroxide (NaOH, 99.9%) and hydrochloric acid (HCl, 38%) were purchased from Merck and Sigma-Aldrich (Germany). Pistachio shell waste and kaolin were obtained from a local supplier. Deionized (DI) water was used throughout all experiments.

2.2 Biochar (BPS) synthesis

First, pistachio shells were washed with water to remove impurities, and then they were boiled in water for 2 h until they lost the yellow essence. After boiling, the pistachio shells were washed again and dried completely in an oven at 100°C for 24 h. The dried pistachio shells were placed in the furnace for 3 h at 650°C under a nitrogen gas environment to obtain the pistachio shell biochar (BPS). The obtained BC was powdered using sieves until a partial size below 125 µm was achieved [16][17][18].

2.3 Zeolite-13X synthesis

Zeolite-13X was synthesized from kaolin using the hydrothermal method. At first, kaolin was washed with deionized water and dried completely at 100°C for 24 h. The dried kaolin was placed in the furnace for 3 h at 700°C, with a heating rate of 5 °C /min, until the calcination process could occur. Then, 5g of metakaolin was added to 35 mL of NaOH solution with a concentration of 3 M and was slowly mixed at 80°C for 2 h for gel formation. After the mentioned time, the gel was added to a Teflon-lined steel autoclave and heated at 95°C for 18 h for Zeolite-13X crystal growth. Finally, the resulting product was washed with deionized water several times until the pH reached 7 and placed in an oven at a temperature of 105°C for 24 h to dry completely [15].

2.4 BPS/Zeolite-13X composite synthesis

The BPS/Zeolite-13X composite was synthesized by the hydrothermal method at different BPS/Zeolite-13X mass ratios (90:10, 70:30, and 50:50). The prepared materials were dispersed in 150 mL of deionized water and stirred at 80 °C for 2 h. The suspension was then transferred into a Teflon-lined autoclave and heated at 100 °C for 15 h. The resulting composite was washed and dried at 100 °C for 24 h [19].

2.5 CO_2 adsorption experiments

As illustrated in Fig. 1, the CO_2 adsorption performance of BPS and the BPS/Zeolite-13X composite was evaluated using a laboratory-scale fixed-bed adsorption system. In each experiment, 1 g of adsorbent was placed in a sample holder suspended inside the adsorption column and connected to an external load cell through a thin wire. The load cell continuously recorded the mass variation of the adsorbent throughout the adsorption process. Before each adsorption experiment, to remove moisture and residual gases, N_2 gas was introduced into the adsorption bed for 30 min earlier than CO_2 [20]. Then, the desired CO_2/N_2 gas mixture was introduced into the adsorption column for 60 min. The experiments were performed at 1 bar pressure, room temperature, and the inlet gas flow rate was adjusted and maintained at 50 mL

min^{-1} by rotameter. During the investigation, the effects of contact time (0-60 min), CO_2 inlet concentration (5-80%), and BPS/Zeolite-13X mass ratio (90:10,70:30, and 50:50) on adsorption efficiency were examined. Finally, the adsorption capacities were calculated using the recorded mass validation data.

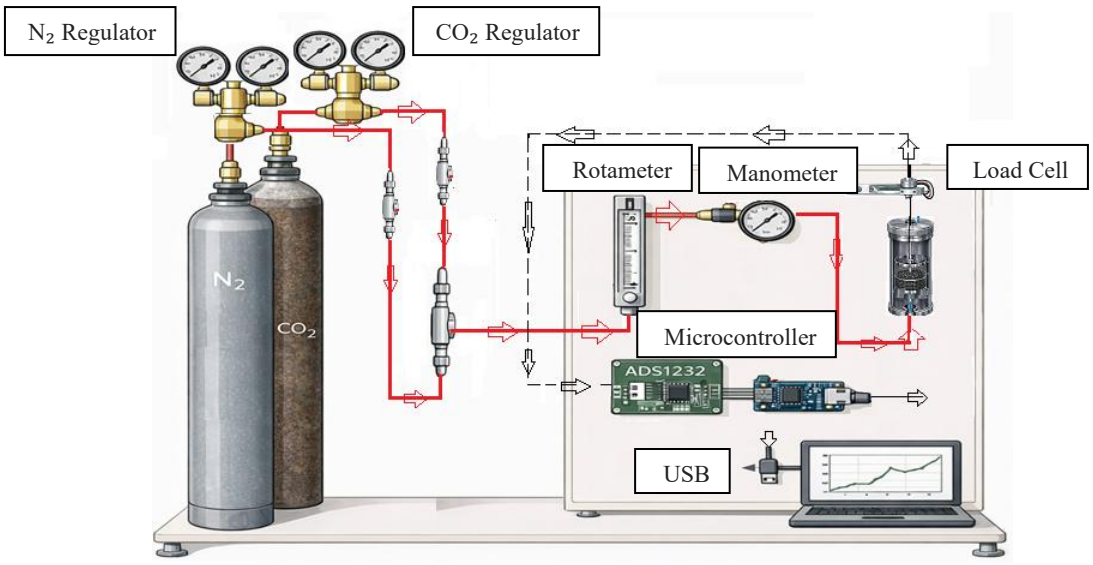


Fig. 1 Schematic illustration of the experimental CO_2 adsorption system.

2.6 Adsorption capacity calculation

The adsorption capacity was determined gravimetrically based on the increase in the adsorbent mass continuously recorded by the load cell during the adsorption process. The equilibrium adsorption capacity (q_e) was calculated according to Eq. (1):

$$q_e = \frac{(m_f - m_i) \times 1000}{M_{CO_2} \times m_{adsorbent}} \quad (1)$$

where q_e (mmol g^{-1}) is the equilibrium adsorption capacity, m_i (g) and m_f (g) are the initial and equilibrium masses of the adsorbent before and after CO_2 adsorption, respectively. M_{CO_2} represents the molar mass of CO_2 (44.01 g mol^{-1}) [21].

3 Results and discussion

3.1 Adsorbent characterization

Fig. 2(a) shows the FTIR spectra of BPS and BPS/Zeolite-13X before CO_2 adsorption process. In the FTIR spectra of BPS, the intense absorption band centered at 3437 cm^{-1} is due to O-H stretching vibration of adsorbed water molecules. The absorption band observed at 2996 cm^{-1} is assigned to C-H stretching vibrations of aliphatic hydrocarbons. The bands centered at 1725 and 1625 cm^{-1} are due to C=O stretching vibrations of carbonyl groups and aromatic C=C stretching vibrations, respectively. The absorption band at 1073 cm^{-1} is due to C-O stretching vibrations [22]. In the FTIR spectra of BPS/Zeolite-13X, the absorption bands centered at

approximately 1001 and 570 cm^{-1} are assigned to Si-O and Al-O stretching vibrations, respectively. The absorption band at approximately 1073 cm^{-1} is due to Si-O-Al framework vibrations, while the bands at 3437 and 1073 cm^{-1} are due to O-H stretching vibrations and C-O stretching vibrations, respectively [15].

FTIR spectra of BPS and BPS/Zeolite-13X are compared in Fig. 2(b). A visual comparison of the FTIR spectra suggests that the characteristic FTIR bands of BPS/Zeolite-13X appeared almost at the same positions before and after CO_2 exposure. However, it was observed that the intensities of some bands decreased upon CO_2 adsorption. In addition, some bands shifted towards higher and lower wavenumbers. It was also noted that new absorption bands did not appear upon CO_2 exposure, indicating that no new functional groups were formed after CO_2 adsorption. It can be concluded that CO_2 exposure did not cause prominent changes in the physicochemical properties of BPS/Zeolite-13X. These observations indicate that physisorption played a dominate role in the CO_2 adsorption process. The absence of new absorption bands suggests that no stable chemical bonds were formed between CO_2 molecules and the adsorbent during the adsorption process [23]. The absence of characteristic carbonate, bicarbonate, or carbamate bands after CO_2 adsorption indicates that stable chemical species were not formed on the adsorbent surface, supporting the predominance of a physisorption mechanism under the studied operating conditions.

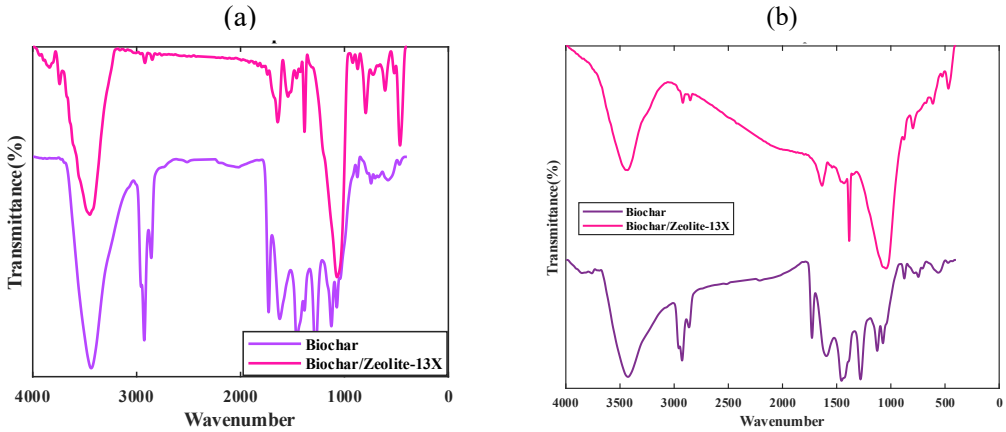


Fig. 2 FTIR spectra of BPS and BPS/Zeolite-13X before and after CO_2 adsorption, (a) before adsorption, (b) after adsorption.

XRD patterns of BPS, Zeolite-13X, and BPS/Zeolite-13X adsorbents are shown in Fig. 3. In the XRD pattern of BPS, a broad peak was observed in the 2θ range of 15 -25°, which can be attributed to the amorphous carbon structure of the biochar [22]. In contrast, in the XRD pattern of Zeolite-13X, diffraction peaks were observed at approximately 10.1°, 11.9°, 15.5°, 18.6°,20.3°, 23.5°, 26.9°, 29.4°, and 30.8°, which confirmed the successful formation of the crystalline zeolite framework [15]. When Zeolite-13X was introduced into the BPS structure, an obvious alteration was observed in the 2θ range of 5-40°, which was attributed to the presence of Zeolite-13X. The presence of the characteristic diffraction peaks of Zeolite-13X in the XRD pattern of the BPS/Zeolite-13X composite confirmed that the crystalline structure of Zeolite-13X was well preserved after composite preparation, indicating its successful incorporation into the biochar matrix [15].

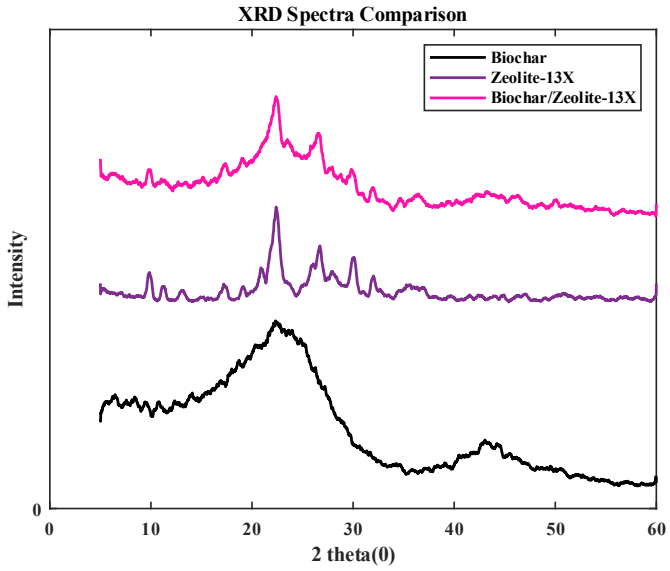


Fig. 3 XRD patterns of BPS, Zeolite-13X, and BPS/Zeolite-13X samples.

According to Fig. 4(a), (b), and (c), the N_2 adsorption/desorption isotherms were measured to evaluate the textural characteristics of BPS, Zeolite-13X, and the BPS/Zeolite-13X composite. The corresponding textural parameters are summarized in Table 1. The surface areas of BPS, Zeolite-13X, and the BPS/Zeolite-13X composite were determined by the BET method and found to be 184.74, 467.79, and 357.05 m^2/g, respectively. It can be seen that the surface area of the composite was enhanced remarkably compared to the initial BPS, which could be ascribed to the introduction of Zeolite-13X with a higher surface area. However, the surface area of the composite was lower than that of Zeolite-13X, which might be related to the low content of Zeolite-13X. The total pore volumes of the composite decreased from 0.216 cm^3/g for BPS to 0.175 cm^3/g for the composite, and the average pore size reduced from 5.577 nm to 2.023 nm. Such changes could be caused by filling some pores in BPS with Zeolite-13X crystals and the reduction in macropores. According to the IUPAC classification, the isotherm of BPS belongs to Type IV, which suggests that BPS consists of mesopores. In contrast, the isotherm of BPS /Zeolite-13X composite exhibits a mixed Type I and Type IV, which implies that the composite contains micropores (dominated by Zeolite-13X) and mesopores (belonging to BPS). The composite with dual pore structure (micropores and mesopores) is supposed to provide more active sites for CO_2 adsorption and a faster diffusion rate of CO_2 molecules [24][25][26][27].

Table 1 Textural properties of BPS, Zeolite-13X, and BPS/Zeolite-13X composite.

Samples	Specific surface area ($m^2\ g^{-1}$)	Total pore volume ($cm^3\ g^{-1}$)	Average pore diameter (nm)
BPS	184.74	0.216	5.577
Zeolite-13X	467.79	0.259	2.265
BPS/Zeolite-13X (70:30)	357.05	0.175	2.023

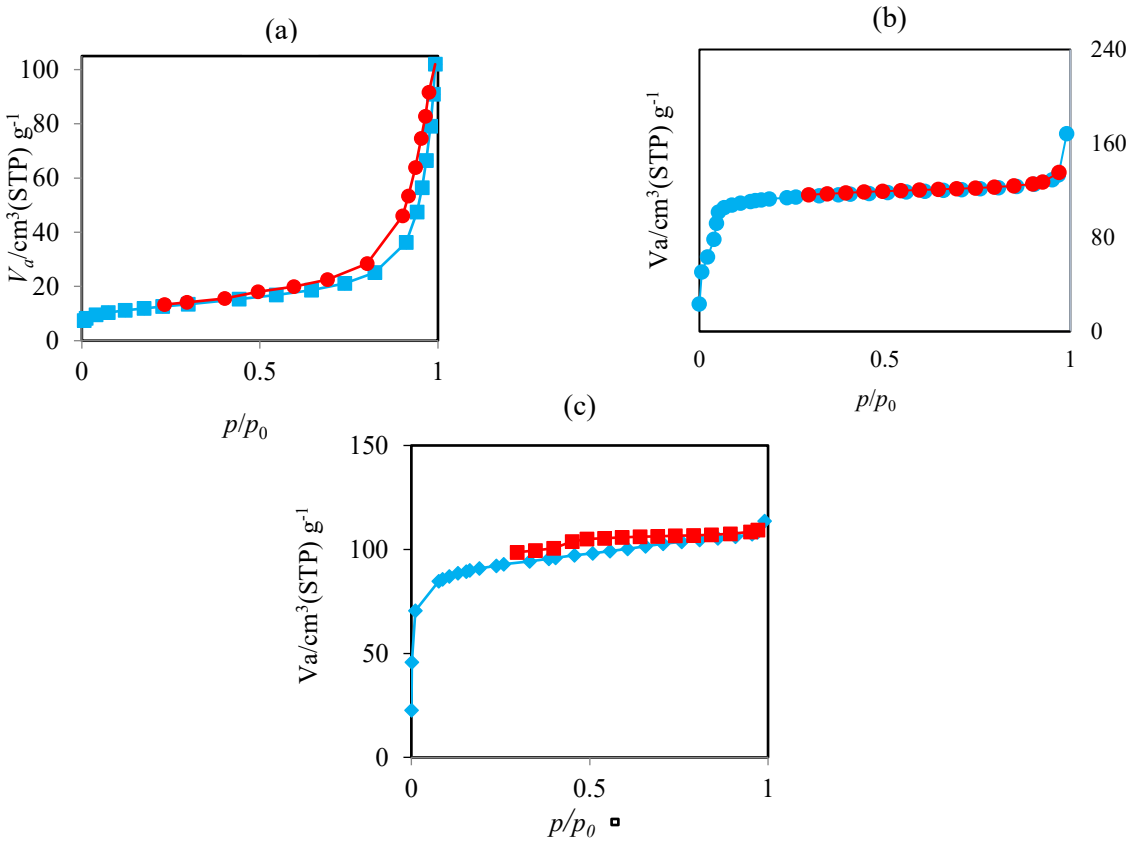


Fig. 4 N_2 adsorption–desorption isotherms of (a) BPS, (b) Zeolite-13X, and (c) BPS/Zeolite-13X composite.

The surface morphological features and elemental composition of the prepared BPS and BPS/Zeolite-13X adsorbents were examined using scanning electron microscopy coupled with energy-dispersive X-ray spectroscopy (SEM–EDX). Fig. 5(a) presents the SEM micrograph of the unmodified BPS, which is characterized by an uneven surface with numerous pores and cavities [23]. In turn, Fig. 5(c) reflects changes in the surface structure of BPS/Zeolite-13X biochar. It could be observed that the surface of the composite material was covered with crystalline particles of Zeolite-13X nano adsorbent, making it irregular and rougher than the initial BPS surface [28]. Thus, it could be concluded that Zeolite-13X particles were successfully attached to the surface of the BPS without damaging its porous structure.

In addition, the elemental composition of the studied materials was determined using EDX analysis, with the results presented in Fig. 5(b) and (d). According to Fig. 5(b), the EDX spectrum of the unmodified BPS contained 92.05% carbon and 7.95% oxygen. At the same time, the modified BPS/Zeolite-13X composite demonstrated the presence of carbon (63.12%), oxygen (17.86%), silicon (2.14%), aluminum (6.42%), and sodium (10.46%), as could be seen from Fig. 5(d). The detection of aluminum, silicon, and sodium in the composition of the modified BPS/Zeolite-13X biochar confirmed its successful modification with Zeolite-13X [29].

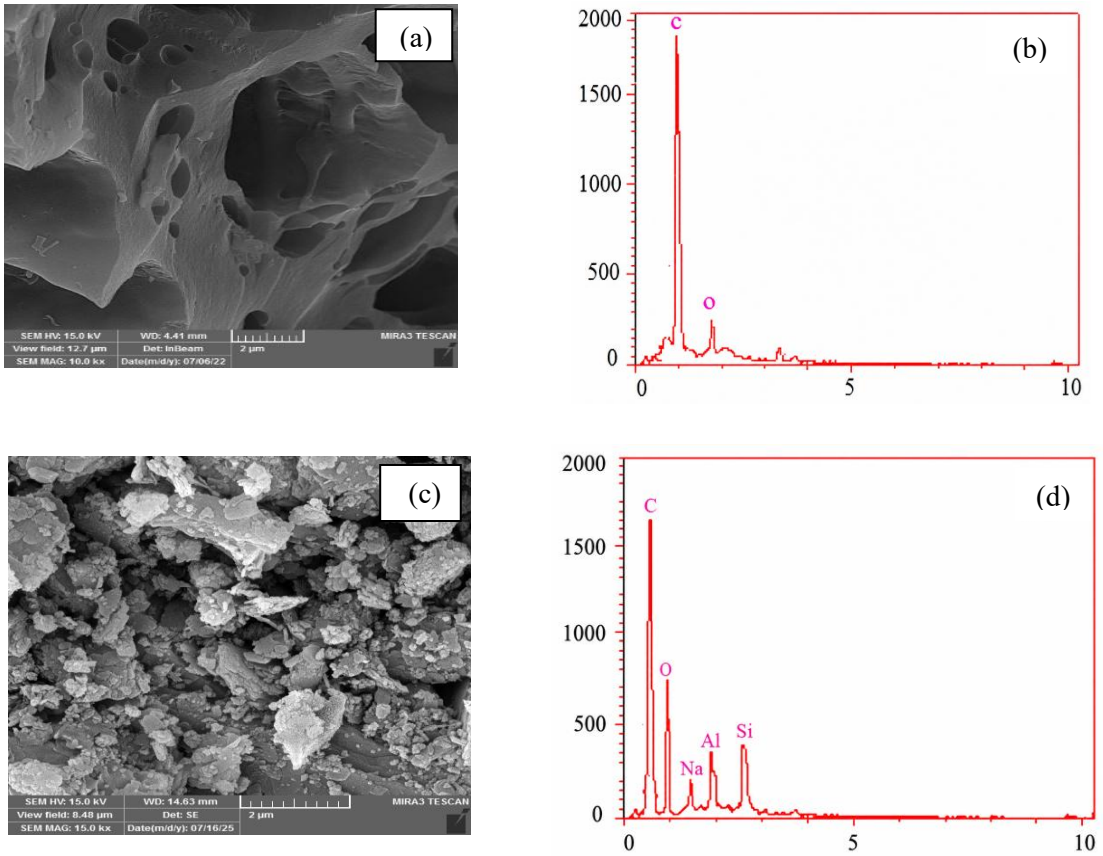


Fig. 5 SEM images and EDX spectra of BPS and BPS/Zeolite-13X adsorbents: (a) SEM image of BPS, (b) EDX spectrum of BPS, (c) SEM image of BPS/Zeolite-13X, and (d) EDX spectrum of BPS/Zeolite-13X.

3.2 Adsorption mechanism

The possible mechanisms of CO_2 adsorption onto the BPS/Zeolite-13X composite through six synergistic interaction pathways are proposed in Fig. 6.

Physically adsorbed CO_2 was mainly controlled by the porous properties of the composite material. Although the addition of Zeolite-13X enhanced the surface area (357.05 m^2/g) compared to the BPS (184.74 m^2/g), the pore volume (0.216 to 0.175 cm^3/g) and pore diameter (5.577 to 2.023 nm) were reduced owing to the partial blocking of the mesopores by the zeolite particles. Indeed, the reduced pore volume and diameter are expected to promote the pore filling mechanism (pathway 4), upon which CO_2 molecules are stored in the micropores and mesopores of the adsorbent [9]. This was evidenced by the SEM and XRD results (Figs. 5 and 3), which showed that Zeolite-13X particles were distributed on the surface of the biochar while retaining their crystallinity (typical peaks at 10.1-30.8°), confirming their role in enhancing the surface area of the composite. Furthermore, dispersion forces (pathway 5) between the CO_2 molecule and the surface of the aromatic carbon skeleton may have contributed to physical adsorption, although their contribution was relatively limited. In particular, the increase in the surface area of the composite (357.05 m^2/g) compared to the surface area of the biochar (184.74 m^2 /g) enhanced the number of active sites available for physisorption.

Meanwhile, oxygen-containing surface groups of the biochar (pathway 6), identified by FTIR analysis as hydroxyl (-OH, 3437 cm^{-1}) and ether (C-O, 1073 cm^{-1}) groups, could participate in weak hydrogen-bonding interactions (pathway 3) with the oxygen atoms of the CO_2 molecule.

The two major interaction pathways that favored enhanced CO_2 uptake capacity of the composite were related to the introduction of Zeolite-13X into the biochar matrix. In particular, Si-O/Al-O symmetric stretching vibrations (1001 cm^{-1}) and Si-O-Al bending vibrations (570 cm^{-1}) were detected by FTIR analysis of the composite, confirming the presence of the aluminosilicate framework of Zeolite-13X. The oxygen atoms associated with the Si-O-Al framework of Zeolite-13X can participate in dipole-quadrupole interactions (pathway 2) with the CO_2 molecule. More importantly, the quadrupole moment of the CO_2 molecule interacted with the exchangeable extra-framework cations (Na^+) present in the pores of Zeolite-13X through electrostatic forces (pathway 1). These electrostatic interactions are generally considered weak physical interactions that induce dipole moments in the CO_2 molecule and temporarily trap it near the cationic sites [30]. This hypothesis was consistent with the EDX results, which showed that the composite contained cations Na^+, Si, and Al distributed over the surface of the material. Notably, the cationic sites in the zeolite pores and oxygen atoms in the Si-O-Al framework of Zeolite-13X contribute to the enhanced CO_2 adsorption capacity through weak electrostatic and dipole-quadrupole interactions.

Experimental evidence for the physisorption mechanism of CO_2 on the composite was provided by the FTIR spectra of the composite and the biochar before and after CO_2 adsorption. In particular, no new absorption peaks were observed after CO_2 adsorption, suggesting that no chemical bonds were formed between the adsorbate and the adsorbent. At the same time, the decrease in the intensity of the absorption peaks, along with their shift, was noticeable for both the composite and the biochar. These results indicated that physical adsorption was the major mechanism of CO_2 capture, consistent with pore filling and dispersion forces that occurred between the adsorbate and the adsorbent [23]. Overall, the present analysis suggests that CO_2 adsorption on the BPS/Zeolite-13X composite was predominantly governed by physisorption through pore filling, electrostatic interactions, dipole quadrupole interactions, weak hydrogen bonding, and dispersion forces. These weak non-covalent interactions enhanced the adsorption performance without the formation of new chemical bonds.

The physisorption mechanism of CO_2 on the composite was further supported by the adsorption isotherm and kinetic model analysis. In particular, the high coefficient of determination of the Sips isotherm ($R^2 > 0.99$) for both adsorbents (BPS/Zeolite-13X: $R^2 = 0.995$; BPS: $R^2 = 0.990$) and the difference in q_m (1.54 mmol/g for BPS/Zeolite-13X and 1.04 mmol/g for BPS) and K_s (9.50 bar^{-1} for BPS/Zeolite-13X and 4.50 bar^{-1} for BPS) suggested the presence of heterogeneous adsorption sites on the surface of the composite [31].

Presumably, pores of different sizes, surface hydroxyl groups capable of weak hydrogen-bonding interactions, and cation-exchange sites contributed to CO_2 adsorption, which was consistent with the FTIR results. Besides, the adsorption process of CO_2 onto the composite and the biochar was better described by the pseudo-second-order (PSO) kinetic model (for BPS/Zeolite-13X and BPS, $R^2 = 0.999$) than by the pseudo-first-order (PFO) kinetic model (for BPS/Zeolite-13X and BPS, $R^2 = 0.991$). In general, the applicability of the PSO model to the experimental data suggested that the adsorption rate was related to the availability of adsorption sites on the adsorbent surface rather than being solely controlled by the concentration of the

adsorbate. According to the PSO kinetic model, the calculated pseudo-second-order rate constant (K_2) and the equilibrium adsorption capacity ($q_{e,\,cal}$) were higher for the composite (K_2 = 0.0869 g·mmol^{-1} ·min^{-1}, $q_{e,\,cal}$ = 1.447 mmol/g) than for the biochar (K_2 = 0.0838 g·mmol^{-1} ·min $^{-1}$, $q_{e,\,cal}$ = 1.032 mmol/g). Although the qe,cal values obtained from the PSO model were somewhat higher than the experimental qe values (qe,exp = 1.237 and 0.869 mmol/g for the composite and biochar, respectively), the higher qe,cal and K_2 values for the composite are consistent with the higher q_m obtained from the Sips isotherm, further supporting the greater number of active adsorption sites available in the composite. Specifically, the composite had a higher CO_2 uptake capacity (q_m = 1.54 mmol/g for the composite and q_m = 1.04 mmol/g for the biochar) and a higher number of active sites for CO_2 adsorption, which was explained by a higher availability of cation-exchange sites and oxygen atoms of the Si-O-Al framework.

Overall, CO_2 adsorption on the BPS/Zeolite-13X composite was predominantly governed by physisorption through pore filling, electrostatic interactions, dipole-quadrupole interactions, weak hydrogen bonding, and dispersion forces. These synergistic interactions enhanced the CO_2 adsorption performance without the formation of new chemical bonds.

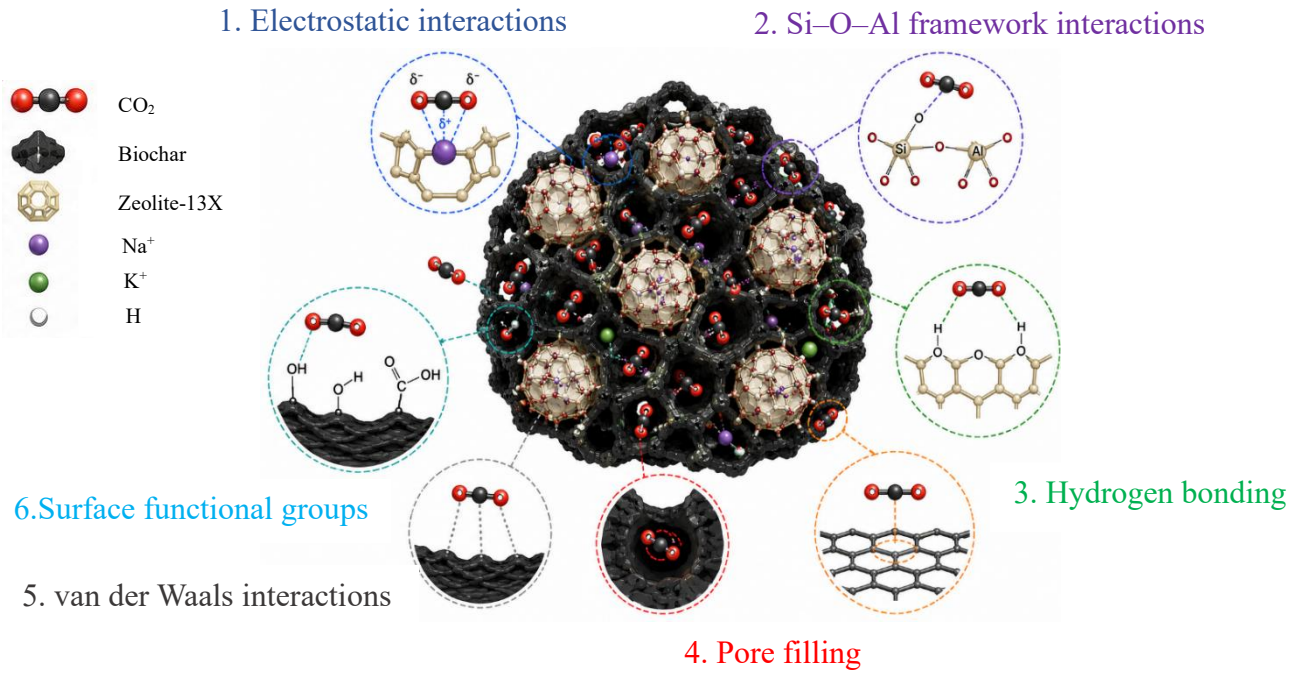


Fig. 6 Proposed mechanism of CO_2 adsorption on the BPS/Zeolite-13X composite.

3.3 Response Surface Methodology (RSM)

The combined influence of CO_2 concentration, BPS/Zeolite-13X mass ratio, and contact time on the adsorption capacity of the adsorbent was studied using Response Surface Methodology (RSM). The statistical analysis and experimental design were performed using Minitab software (Version 20, Minitab LLC, State College, PA, USA). A second-order polynomial equation was used as a model function to describe the relationship between the independent variables and the response variable. The adequacy and significance of the developed model

were checked by performing the analysis of variance (ANOVA). In addition, the model was evaluated using regression analysis, residual plots, and optimization criteria [27].

Table 2 Analysis of variance (ANOVA) for the developed quadratic model.

Source	DF	Adj SS	Adj MS	F	P	Sig.
Model	9	2.4498	0.27221	46.638	5.445×10^{-7}	***
Linear	3	1.4027	0.46757	80.112	2.707×10^{-7}	***
Nonlinear	6	1.0471	0.17452	29.902	7.873×10^{-6}	***
Residual	10	0.058365	0.0058365	-	-	-
Lack of fit	5	0.058214	0.011643	384.67	1.8546×10^{-6}	***
Pure error	5	0.00015133	3.0267×10^{-5}	-	-	-
Total	19	2.5082	-	-	-	-

As listed in Table 2, the produced quadratic model was significant because the model F-value was 46.64, whereas the p-value was less than 0.0001, suggesting that the suggested quadratic regression model was adequate to represent the adsorption data [32]. Indeed, the goodness of fit for the regression model was supported by a high coefficient of determination ($R^2 = 0.9767$), which indicates that 97.67% of the variance can be explained by the produced model. Besides, since the adjusted R^2 (0.9558) and predicted R^2 (0.8247) were in concordance with the coefficient of determination, and the root mean square error (RMSE) was only 0.0764 mmol. $g^{-1;}$ this suggests that the developed quadratic model was accurate to predict adsorption capacity [33] (Table 2).

Table 3 Estimated regression coefficients of the quadratic model.

Term	Estimate	SE	t	P	Sig.
CO_2	0.013858	0.003938	3.5191	0.00555	**
Biochar	0.033385	0.016323	2.0453	0.06804	ns
Time	0.031503	0.005491	5.7368	0.00019	***
CO_2×Time	6.9469E-05	2.6066E-05	2.6651	0.02369	*
CO_2^2	-1.0974E-04	3.4313E-05	-3.1981	0.00952	**
Time²	-3.6595E-04	6.1496E-05	-5.9507	0.00014	***

The estimated regression coefficients of the quadratic model are presented in Table 3. Statistically significant positive linear effects of CO_2 concentration and contact time on the response variable were observed. The interaction between CO_2 concentration and contact time also had a statistically significant positive effect on the adsorption capacity. However, the interaction between CO_2 concentration and BPS/Zeolite-13X mass ratio, as well as the interaction between BPS/Zeolite-13X mass ratio and contact time were found to be statistically insignificant ($p>0.05$) [34] (Table 3). The quadratic terms for CO_2 concentration and contact time were found to be significant, suggesting a nonlinear relationship between these variables and the response variable [35].

The final quadratic regression equation is given as follows:

q_{eq} = -1.154002 + 0.013858 (CO_2) + 0.033385 (Biochar) + 0.031503 (Time) - 7.1863×10^{-6} (CO_2 × Biochar) + 6.9469×10^{-5} (CO_2 × Time) - 1.1413×10^{-5} (Biochar × Time) - 1.0974×10^{-4} (CO_2^2) - 2.4370×10^{-4} (Biochar²) - 3.6595×10^{-4} (Time²)

The obtained regression equation can be used to estimate the adsorption capacity in the experimental region correctly. The positive values of linear coefficients indicate that the increase of these variables leads to the growth of the CO_2 adsorption capacity [36], while the negative value of the quadratic coefficient implies the existence of optimum conditions in the experimental range [37].

3.3.1 Response surface and contour analysis

The three-dimensional response surface and the contour plots were drawn to demonstrate the combined effect of the independent variables on the response (q_{eq}), and also to visualize the relationship between the parameters and indicate the optimum region [33].

Fig. 7(a) presents the response surface and contour plot for CO_2 concentration and BPS/Zeolite-13X mass ratio with the center point of contact time. An increase in CO_2 concentration resulted in a gradual increase in Adsorption capacity. It means that increasing the driving force from the CO_2 concentration gradient led to enhanced CO_2 adsorption [38]. The response surface showed an increasing trend with increasing BPS/Zeolite-13X mass ratio. Nevertheless, the influence of the second variable was less compared to the first one [24]. Moreover, the response surface had a slight curvature, suggesting the non-linear nature of the relationship. On the other hand, the interaction between variables was minimal, which was also supported by the statistical analysis [33]. For example, a high adsorption capacity was detected for high CO_2 concentration and moderate and high values of the BPS/Zeolite-13X mass ratio.

Fig. 7(b) presents the effect of contact time and the CO_2 concentration on the adsorption capacity at a fixed level of the biochar sample. The response surface plot indicates that both parameters have positive effects on the adsorption capacity since the surface increases progressively with an increase in either of the factors. Moreover, the Fig. 7(b) shows that the curve has a non-zero curvature, suggesting that the quadratic model is appropriate for the experimental data because it considers the squared terms. The contour plot of Fig. 7(b) depicts an elliptical shape that reveals that the interaction effect between CO_2 concentration and contact time is significant, which coincides with the results of Table 2 [39]. According to Fig. 7(b), the adsorption capacity reaches a maximum at high levels of CO_2 concentration and contact time, which can be explained by the fact that both factors affect the adsorption driving force and increase the adsorption equilibrium time [40].

Fig. 7(c) presents the interaction effect between the two factors (BPS/Zeolite-13X mass ratio and contact time) at the central level of the CO_2 concentration. It can be observed that increasing the contact time resulted in an increase CO_2 adsorption capacity. The effect of contact time was more considerable than the effect of BPS/Zeolite-13X mass ratio [41].

This conclusion can be drawn from the given regression equation. In particular, a linear increase in adsorption capacity was observed with respect to contact time, which is explained

by the high p-value (0.001). However, the linear effect of the BPS/Zeolite-13X mass ratio was not significant, indicating that this parameter did not significantly influence the CO_2 adsorption capacity at a 95% confidence level. Thus, the contour plot reflects this result since the response surface is flat and the lines are far apart. This indicates that changes in contact time have a more significant effect on the response variable. [39].

In general, the three-dimensional response surfaces revealed that CO_2 concentration and contact time were the most influential factors affecting the equilibrium adsorption capacity. The response surfaces illustrated the non-linear behavior of the adsorption process, while statistical analysis indicated insignificant interaction effects involving the BPS/Zeolite-13X mass ratio. Thus, the quadratic model was found to be appropriate for describing the experimental data. The contour plots showed the optimal region for achieving the highest predicted adsorption capacity, which was associated with high CO_2 concentrations and long contact times [42][43].

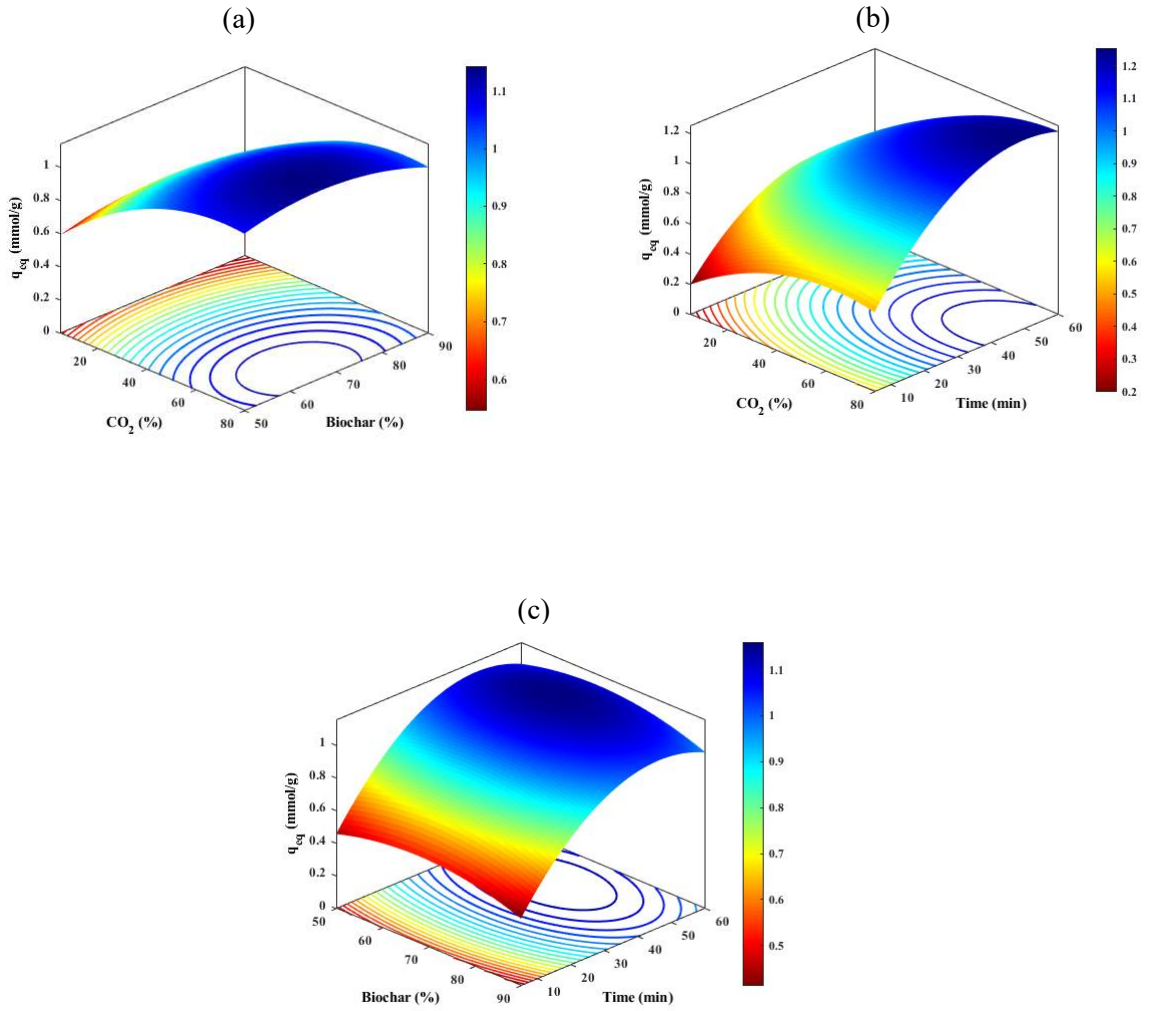


Fig. 7 Three-dimensional response surface plots showing the effects of (a) BPS/Zeolite-13X mass ratio and CO_2 inlet concentration, (b) contact time and CO_2 inlet concentration, and (c) contact time and BPS/Zeolite-13X mass ratio on CO_2 adsorption capacity.

3.3.2 Main effects analysis

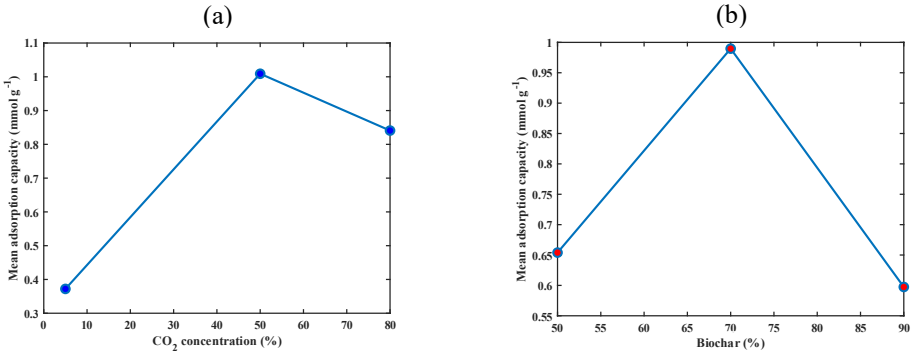
The main effects plot of CO_2 concentration, BPS/Zeolite-13X mass ratio, and contact time on the adsorption capacity is displayed in Fig. 8. It should be noted that the influence of each operating variable on the response was visualized by the average response values at the particular value of the given variable while the other factors were kept constant [33].

As seen in Fig. 8(a), the CO_2 concentration demonstrated the highest impact on the adsorption performance. Indeed, the increase in CO_2 concentration from 5% to 80% led to a significant increment in the average adsorption capacity. This behavior can be explained by the fact that higher CO_2 concentrations provide higher partial pressures of CO_2, resulting in higher driving forces for CO_2 diffusion and, consequently, higher uptake by the composite adsorbent [44].

The main effect of the BPS/Zeolite-13X mass ratio on the adsorption capacity is illustrated in Fig. 8(b). It was found that increasing the BPS/Zeolite-13X mass ratio to the intermediate level (70:30) increased adsorption capacity. At the same time, no significant difference in adsorption capacity was observed between the higher levels of the BPS/Zeolite-13X mass ratio. It can be concluded that an optimal balance between the porous structure of the biochar and the ionic exchange capacity of zeolite should be determined to maximize the adsorption capacity [45]. Although the intermediate level of the BPS/Zeolite-13X mass ratio showed the best results in terms of adsorption capacity, the linear trends showed no significant ($P > 0.05$) independence, implying that the main effect of the BPS/Zeolite-13X mass ratio was less significant compared to the effect of other variables.

Finally, the main effect of the contact time on the adsorption capacity is demonstrated in Fig. 8(c). As expected, the adsorption capacity increased with an increase in the contact time due to additional CO_2 molecules' diffusion into the pores of the adsorbent. However, the adsorption capacity trends showed that after 50 min, no significant difference in the adsorption capacity was observed at different contact times. The reason for this trend can be explained by the adsorbent's pore structure properties, which can limit the adsorption process and cause the adsorption equilibrium [46].

Thus, the graphical analysis of the main effect plots indicated that the CO_2 concentration showed the highest impact on the adsorption capacity, while the contact time demonstrated the secondary influence. The BPS/Zeolite-13X mass ratio revealed no significant trends in the adsorption capacity at different levels of the given factor. The observed trends correspond to the results of the ANOVA analysis, which showed that CO_2 concentration and contact time were statistically significant factors, whereas the linear effect of the BPS/Zeolite-13X mass ratio was not significant at the 95% confidence level.



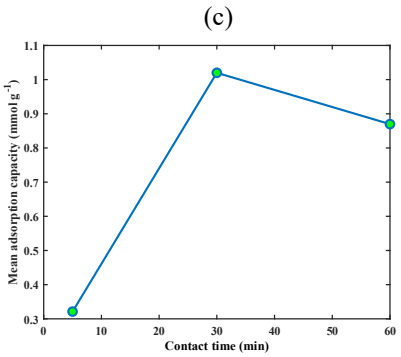


Fig. 8 Main effects plots illustrating the influence of (a) CO_2 concentration, (b) BPS/Zeolite-13X mass ratio, and (c) contact time on the CO_2 adsorption capacity.

3.3.3 Model validation

The comparison between the experimental adsorption capacities and model responses is presented in Fig. 9. It can be seen that most of the data points were close to the 45° reference line, indicating that predicted responses were consistent with the observed ones. This indicate that the developed model provides reliable predictions within the investigated experimental domain. A high determination coefficient (R^2 = 0.9767) also confirms this statement [42][47].

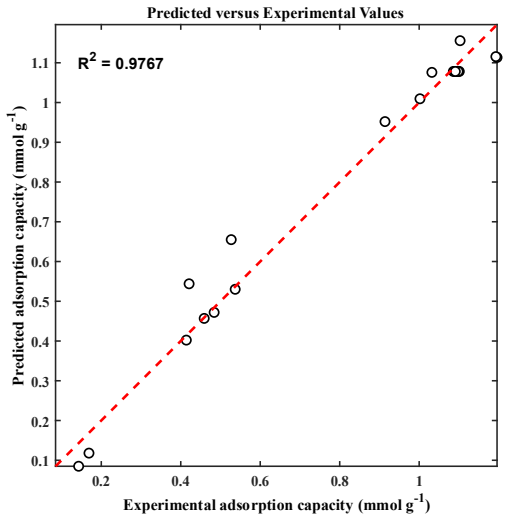


Fig. 9 Comparison between the predicted and experimental adsorption capacities obtained from the developed RSM model.

3.3.4 Numerical optimization

Numerical optimization of the developed quadratic response surface model was carried out to identify the operating conditions under which the maximum CO_2 adsorption capacity can be achieved within the investigated experimental domain. The optimization of the CO_2 adsorption capacity was performed by maximizing the adsorption capacity while keeping all other process variables within the experimental domain considered in this study [33].

Table 4 Optimum operating conditions and predicted maximum CO_2 adsorption capacity obtained using response surface methodology (RSM).

Parameter	Optimum value
CO_2 concentration (%)	76.57
BPS/Zeolite-13X mass ratio	66.21:33.79
Contact time (min)	49.28
Predicted adsorption capacity (mmol g^{-1})	1.258
Overall desirability	1.000

The optimum operating conditions predicted by the response surface methodology are presented in Table 4 According to the model, the maximum adsorption capacity was 1.258 mmol g^{-1}, which was achieved at 76.57% CO_2 concentration, a BPS/Zeolite-13X mass ratio of 66.21:33.79, and a contact time of 49.28 min. A desirability value of 1.000 indicated that the obtained operating conditions were optimum and satisfied all the specified criteria [33].

To further verify the predictive ability of the obtained model, an independent adsorption experiment was carried out using 80% CO_2 concentration, a BPS/Zeolite-13X mass ratio of 70:30, and 60 min contact time. As a result, the adsorption capacity was found to be 1.237 mmol g^{-1}.

Table 5 Comparison between the predicted optimum response and the independent experimental validation.

Condition	CO_2 (%)	BPS/Zeolite-13X mass ratio	Time (min)	Adsorption capacity (mmol g^{-1})
RSM prediction	76.57	66.21:33.79	49.28	1.258
Experimental validation (mean ± SD, n = 3)	80	70:30	60	1.237± 0.029

As shown in Table 5, the experimental adsorption capacity was found to be very close to the maximum adsorption capacity predicted by the RSM model. To validate the developed RSM model, the optimum operating conditions predicted by the model were experimentally examined in triplicate. The comparison between the experimental and predicted CO_2 adsorption capacities at the optimum condition is presented in Fig. 10. The average experimental CO_2 adsorption capacity was 1.237 ± 0.029 mmol g^{-1} (n = 3), which was in close agreement with the RSM-predicted value of 1.258 mmol g^{-1}, thereby confirming the reliability and predictive capability of the developed model. Even though the operating conditions used in the experiments were not exactly those predicted by the numerical optimization, the difference between the predicted and experimentally measured values was insignificant. These results indicate that the quadratic model is satisfactory, robust, and accurate enough to describe the CO_2 adsorption process within the studied experimental domain. Thus, the developed RSM model was demonstrated to be appropriate for further applications in the prediction and optimization of the CO_2 adsorption capacity [33].

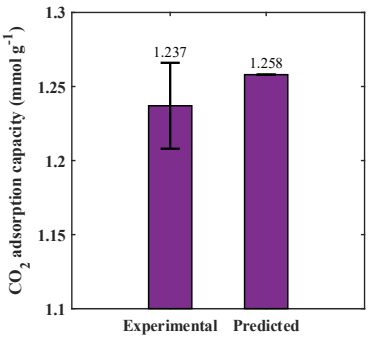


Fig. 10 Comparison of experimental and predicted CO_2 adsorption capacities at the optimum condition. Error bars represent the standard deviation of experimental measurements.

3.4 Adsorption kinetics

In this study, to better understand the adsorption behavior and rate-controlling mechanism of CO_2 adsorption onto BPS and BPS/Zeolite-13X adsorbents, the pseudo-first-order (PFO) and pseudo-second-order (PSO) kinetic models were applied to the experimental data obtained over an adsorption period of 60 min. The nonlinear forms of the PFO and PSO kinetic models are presented in Eqs. (2) and (3), respectively [48][49][50].

$$q_t = q_e(1 - e^{-K_1 t}) \tag{2}$$

$$q_t = (K_2 q_e^2 t) \,/\, (1 + K_2 q_e t) \tag{3}$$

The best-fitted pseudo-first-order (PFO) and pseudo-second-order (PSO) kinetic models for CO_2 adsorption onto BPS and BPS/Zeolite-13X are presented in Table 6, while the corresponding non-linear fitting curves of the experimental data are presented in Fig. 11(a) and (b), respectively. The results presented in Table 6 demonstrate that the correlation coefficient (R^2) for PSO was found to be slightly higher (0.99906 for BPS and 0.99903 for BPS/Zeolite-13X) compared to that of the PFO model for the adsorption of CO_2. This observation implies that the PSO kinetic model has a better fit to the experimental data in comparison to the PFO kinetic model. The CO_2 adsorption kinetic were better described by the PSO kinetic model, indicating that the adsorption process was influenced by the availability of active adsorption sites. However, it should be noted that the surface-controlled mechanism does not necessarily imply chemisorption of CO_2 molecules onto the surface of the adsorbent. Therefore, the satisfactory fitting of the PSO model should be interpreted as evidence of adsorption kinetics controlled by the availability of active adsorption sites rather than direct evidence of chemisorption. Additionally, it can be concluded from Table 6 that the equilibrium adsorption capacity of the BPS/Zeolite-13X composite was found to be comparatively higher than that of the pristine BPS, which confirms that the addition of Zeolite-13X into the BPS matrix improved the CO_2 adsorption capacity of the biochar-based adsorbent [31][51][45]. This interpretation is further supported by FTIR analysis, as evidenced by the FTIR spectra shown in Fig. 2, where no new characteristic peaks emerged after CO_2 adsorption; instead, only shifts in existing peaks were observed, suggesting that CO_2 adsorption was primarily governed by weak interactions (e.g., electrostatic or physical interactions) rather than strong chemisorptive bonding.

Table 6 Variables of the desired kinetic models for the adsorption process of CO_2 gas using the desired adsorbents.

Kinetic model	BPS	BPS/Zeolite-13X
PFO		
$q_{e.cal}$	0.847	1.2341
K_1	0.07892	0.10409
R^2	0.99079	0.99069
PSO		
$q_{e.cal}$	1.0316	1.4471
K_2	0.08379	0.08688
R^2	0.99906	0.99903

(b)

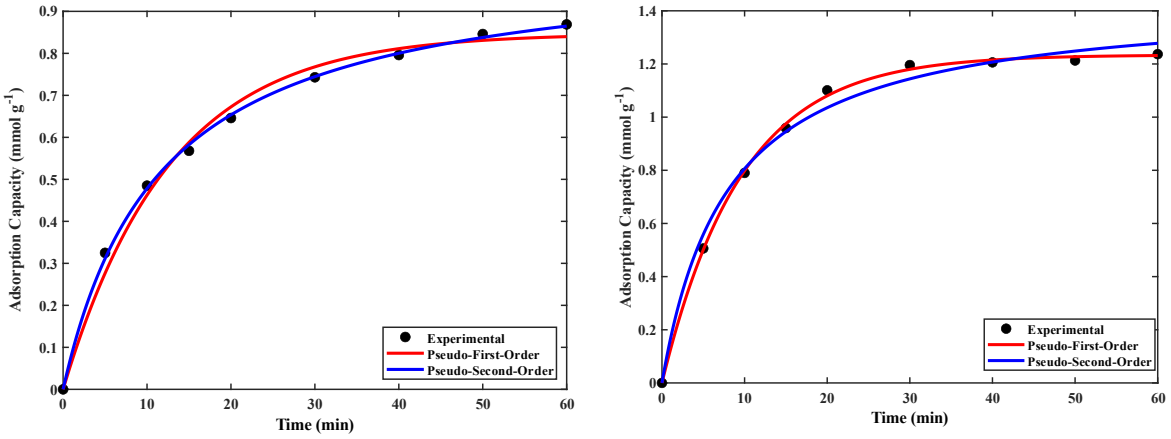


Fig. 11 Nonlinear fitting curves of the pseudo-first-order (PFO) and pseudo-second-order (PSO) kinetic models for CO_2 adsorption onto (a) BPS and (b) BPS/Zeolite-13X adsorbents.

3.5 Adsorption isotherm study

The adsorption isotherm study was conducted to investigate the relationship between the equilibrium CO_2 adsorption capacity and CO_2 concentration, and to evaluate the surface heterogeneity and adsorption behavior of the BPS and BPS/Zeolite-13X adsorbents. The Sips and Toth isotherm models, expressed by Eqs. (4) and (5), were applied to describe the experimental equilibrium data [15].

$$q_e = \frac{q_m(K_S C_e^{1/n})}{1+K_S C_e^{1/n}} \tag{4}$$

$$q_e = \frac{q_m(K_T C_e)}{(1+(K_T C_e)t)^{1/t}} \tag{5}$$

the isotherm parameters and constants for CO_2 adsorption on the studied adsorbents are presented in Table 7. The adsorption data were fitted with the Sips and Toth models, from which the parameters were estimated by nonlinear regression. As shown by the graphs in Fig. 12 (a) and (b), the two models exhibit adequate agreement with the experimental data, and the corresponding curves closely followed the trends of the experimental data points. Nevertheless, the Sips model demonstrated slightly higher R^2 values for both adsorbents, suggesting that the Sips model was more appropriate to fit the adsorption data of CO_2 on the studied materials.

This assumption is supported by the fact that the Sips model considers the heterogeneous nature of surfaces, which was supported by the n_s values being lower than unity, indicating surface heterogeneity. Additionally, a slightly higher q_m was predicted by the model for the composite than for the pristine biochar, which can be seen as an indicator of the beneficial effect of Zeolite-13X addition on CO_2 adsorption capacity. Indeed, the value of this parameter increased by 50% for the composite, reaching 1.54 mmol g^{-1}. On the other hand, the theoretical value of q_m was found to be slightly higher than the corresponding experimental value, which can be explained by the ideal conditions postulated by the model in comparison to practice.

Another important observation was that the affinity constants were higher for the composite, which suggests that the addition of Zeolite-13X increased the affinity of the adsorbent for CO_2 molecules. Overall, the higher qm and affinity constant values of the composite confirmed the positive effect of Zeolite-13X incorporation on CO_2 adsorption performance, which can be attributed to the increased number of available adsorption sites and the synergistic interaction between biochar and zeolite [31][52][53].

Table 7 Variables of the desired isotherm models for the adsorption process of CO_2 gas using the desired adsorbents.

Model	Parameters	Adsorbent		
			BPS	BPS/Zeolite13X
	Sips	q_m (mmol/g)	1.04	1.54
		K_S (bar^{-1})	4.50	9.50
		n_s	0.71	0.73
		R^2	0.990	0.995
	Toth	q_m (mmol/g)	1.02	1.60
		K_T (bar^{-1})	11.02	23.13
		t	0.68	0.62
		R^2	0.989	0.993

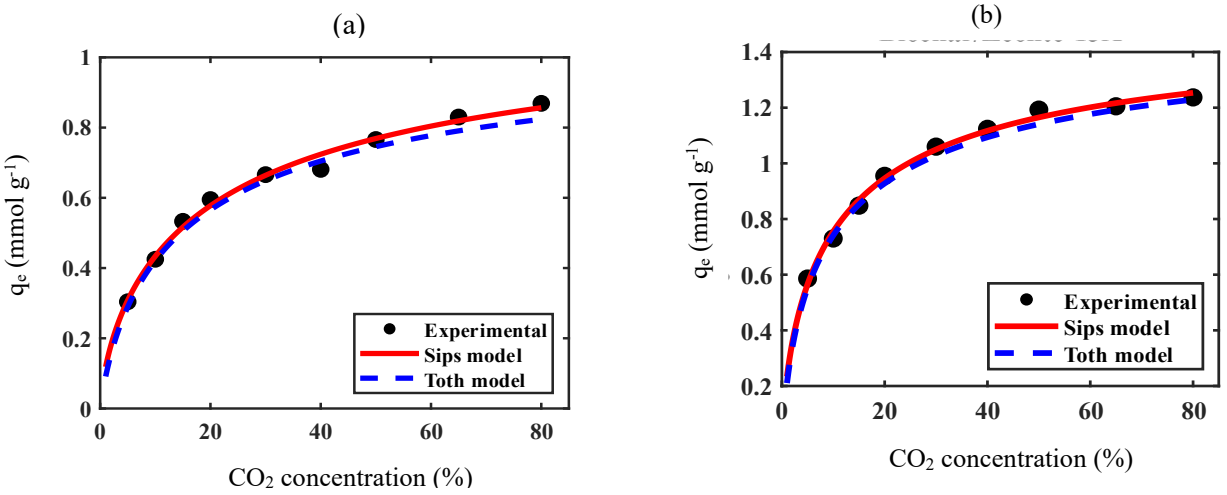


Fig. 12 *Nonlinear fitting curves of the Sips and Toth isotherm models for CO_2 adsorption onto (a) BPS and (b) BPS/Zeolite-13X adsorbents.*

3.6 Comparison with previous studies

To further evaluate the performance of the synthesized adsorbents, the CO_2 adsorption capacities of BPS and the BPS/Zeolite-13X composite were compared with previously reported adsorbents under similar experimental operating conditions (ambient temperature and 1 bar), as summarized in Table 8.

Table 8 Comparison of CO_2 adsorption capacity of biochar, zeolite-13X, and related composites under near-ambient conditions.

Adsorbent	Modification	Temp.	Pressure	CO_2 Capacity (mmol/g)	Reference
KOH-activated biochar (BC)	KOH-activated	25 °C	1 bar	0.59 – 0.88	[9]
Sono-aminated activated biochar (500 °C pyrolysis)	Amine-activated	Ambient	1 bar	0.86 – 1.23	[54]
Sawmill residue biochar	Raw / unmodified	~20 °C	1 bar	2.40	[55]
Commercial zeolite 13X	Raw / unmodified	~20 °C	1 bar	1.70	[55]
Zeolite 13X (from coal-fired slag)	Raw / unmodified	25 °C	1 bar	3.69 (fresh) / 3.37 (10 cycles)	[56]
PEI-modified zeolite 13X (20 wt %)	PEI (amine)-modified	25 °C	1 atm	~1.00	[57]
PEI-modified zeolite 13X (60 wt %, optimum)	PEI (amine)-modified	75 °C	1 atm	1.22	[57]
KOH-activated bamboo biochar	KOH-activated	25 °C	1 bar	3.49	[58]
Pine-derived biochar (800 °C carbonization)	Thermally activated	~30 °C	1 bar	3.50	[59]
N, P co-doped cornstalk biochar	N, P chemically doped	25 °C	1 bar	3.11	[60]
Activated biochar (general)	Chemically activated	25 °C (298 K)	1 bar	>2.35	[9]
Coffee-ground biochar	Raw / unmodified	25 °C	1 bar	2.80	[61]
Biochar (pistachio shell)	Raw / unmodified	25 °C	1 bar	0.869	This work
BPS/Zeolite 13X composite (70:30)	Unmodified (no activation/amine)	25 °C	1 bar	1.237	This work

To assess the performance of the prepared adsorbents, the CO_2 uptake capacities of BPS and the BPS/Zeolite-13X composite were compared with previously reported biochar and Zeolite-13X-based adsorbents under near-ambient conditions, as presented in Table 8. As seen from the comparative analysis, the majority of the works reporting high CO_2 uptake capacities utilized either activated biochar (e.g., KOH activated biochar) [9] [58] or amine-functionalized materials (e.g., PEI impregnated) [54] [57] for CO_2 capture, which generally require complicated and energy-consuming activation or modification steps and/or involve the use of expensive chemicals. On the contrary, the BPS was prepared by a simple pyrolysis of the pistachio shell at 650 °C under N_2 flow without any chemical activation and demonstrated a reasonable CO_2 uptake capacity of 0.869 mmol/g. Moreover, the physical compositing of BPS with Zeolite-13X without any activation or chemical modification led to a significant increase in CO_2 uptake capacity, reaching 1.237 mmol g^{-1}, which represents a 42% improvement compared with pristine BPS.

The primary objective of the present study was not merely to maximize the CO_2 adsorption capacity, but to develop a low-cost and readily accessible biochar-based adsorbent from an

alternative agricultural waste precursor through a simple preparation strategy. To the best of our knowledge, pistachio shell-derived biochar has not been previously investigated for CO_2 capture [62]. Therefore, this study introduces a new biomass-derived precursor and demonstrates that its adsorption performance can be enhanced through a simple physical modification with Zeolite-13X without chemical activation or amine functionalization. This preparation strategy reduces the need for additional chemical reagents and simplifies the fabrication process while utilizing an abundant agricultural residue as the carbon source. Although the CO_2 adsorption capacity of the BPS/Zeolite-13X composite (1.237 mmol g^{-1}) was lower than that reported for some highly engineered adsorbents, such as pristine Zeolite-13X synthesized from coal-fired slag (3.69 mmol g^{-1}) [56], the developed composite exhibited a remarkable 42% improvement compared with pristine BPS. These results highlight the potential of the proposed material as a cost-effective biochar-based adsorbent, particularly for applications where feedstock availability, preparation simplicity, and reduced chemical requirements are important considerations.

The enhanced CO_2 adsorption performance can be attributed to the modified textural properties of the BPS/Zeolite-13X composite, as confirmed by BET analysis. A considerable increase in the surface area (SA) was observed for the composite (357.05 m^2/g), as compared to the initial BPS (184.74 m^2/g). At the same time, the total pore volume (PV) decreased from 0.216 to 0.175 cm^3/g, and the average pore diameter (APD) significantly decreased from 5.577 to 2.023 nm. The significant reduction in APD suggests that the introduction of Zeolite-13X into the BPS matrix altered the pore size distribution, which may be associated with partial occupation of larger pores by zeolite nanoparticles. Previous studies have demonstrated that narrow micropores play an important role in CO_2 adsorption at low pressure and room temperature. Therefore, the presence of microporous regions originating from Zeolite-13X, together with the remaining mesoporous structure of BPS, may contribute to the enhanced CO_2 uptake capacity of the BPS/Zeolite-13X composite.

The possible contribution of narrow pores to CO_2 storage is supported by the adsorption isotherms and kinetic analyses. Indeed, a reasonable agreement between the experimental and calculated data was observed for both Sips and Toth isotherm models with $R^2 > 0.98$, indicating that the CO_2 adsorption process follows both heterogeneous surface energy distribution and nonideal behavior. The highest q_m was found for the BPS/Zeolite-13X composite (1.54–1.60 mmol/g), which is 42% higher than that of pristine BPS (1.02–1.04 mmol/g). Similar results were obtained for the PSO and PFO kinetic models; in particular, a better fit of the experimental data ($R^2 = 0.999$) was found for the PSO model, indicating that the adsorption rate was mainly governed by the availability of active adsorption sites rather than providing direct evidence of chemisorption. This interpretation is consistent with the FTIR results, which showed no formation of new chemical bonds after CO_2 adsorption. Overall, although the CO_2 adsorption capacity of the BPS/Zeolite-13X composite (1.237 mmol g^{-1}) was lower than that of some highly engineered adsorbents, such as activated or chemically modified materials, the developed composite offers several practical advantages. The material was prepared from renewable pistachio shell waste through a simple physical compositing method without chemical activation or amine functionalization, which reduces preparation complexity and chemical consumption. Furthermore, the incorporation of Zeolite-13X significantly enhanced the CO_2 uptake capacity of pristine BPS, demonstrating that a simple and environmentally

friendly modification strategy can effectively improve the adsorption performance of biomass-derived adsorbents under ambient conditions [9] [54] [57] [58] [60].

4 Conclusion

In this paper, a new BPS/Zeolite-13X composite was successfully synthesized through pyrolysis of pistachio shell followed by physical modification of the obtained biochar with Zeolite-13X particles. It was demonstrated that the produced composite exhibited a well-developed porous structure suitable for CO_2 adsorption, as confirmed by SEM and BET analyses, which revealed an improved surface morphology and an increased specific surface area. The FTIR results demonstrated the presence of oxygen-containing functional groups in the biochar and characteristic Si–O–Al vibrations of the Zeolite-13X framework, which can contribute to CO_2 adsorption through weak surface interactions.

The BPS/Zeolite-13X composite exhibited enhanced CO_2 adsorption performance compared with pristine BPS. Under the experimental conditions providing the highest adsorption capacity, the equilibrium CO_2 adsorption capacities of BPS and the BPS/Zeolite-13X composite were 0.869 and 1.237 mmol g^{-1}, respectively. For the BPS/Zeolite-13X composite, this adsorption capacity was obtained at 80% CO_2 concentration, a BPS/Zeolite-13X mass ratio of 70:30, and 60 min contact time. These results indicate that the incorporation of Zeolite-13X into pistachio shell biochar increased its adsorption capacity by approximately 42%. The adsorption kinetics were best described by the pseudo-second-order (PSO) kinetic model, suggesting that the adsorption rate depended on the availability of active adsorption sites rather than providing direct evidence of chemisorption. The equilibrium data for both adsorbents were best fitted by the Sips isotherm model, indicating heterogeneous adsorption behavior with a combination of Langmuir- and Freundlich-type characteristics.

Overall, modification of BPS with Zeolite-13X particles improved the adsorption performance of the original material. The obtained BPS/Zeolite-13X composite demonstrated promising potential as a biomass-derived CO_2 adsorbent. Since this material is derived from inexpensive and readily available agricultural waste, it could provide a cost-effective approach for CO_2 capture. However, further investigations regarding regeneration ability, selectivity, and performance under realistic conditions are required before practical application.

5 Limitations

While the presented manuscript demonstrated the potential of BPS/Zeolite-13X as an adsorbent for CO_2 at ambient temperature and 1 bar, several disadvantages should be noted. Firstly, the CO_2/N_2 selectivity of the developed adsorbent was not studied. This characteristic is of particular importance since in practice, this adsorbent will be used in a mixture of gases such as flue gas or air. Secondly, the stability and regeneration performance of the adsorbent were not investigated; therefore, the optimal desorption temperature and regeneration conditions have not yet been determined, while the decrease in adsorption capacity after multiple adsorption/desorption cycles remains unknown. Although it is known that for the commercial zeolite 13X, regeneration conditions are associated with high temperatures, the choice of mild conditions for this composite material may be justified. However, for practical implementation, it is necessary to know regeneration conditions and the number of cycles of the adsorbent. It would be of interest to study the selectivity of CO_2 separation for BPS/Zeolite-13X in a mixture

of gases such as flue gas and air, as well as its stability and selectivity during multiple adsorption/desorption cycles.

Declaration of competing interest

The authors declare that they have no known competing financial interests or personal relationships that could have appeared to influence the work reported in this paper.

Data availability statement

The data supporting the findings of this study are available from the corresponding author upon reasonable request.

Acknowledgments

The authors would like to express their sincere gratitude to Dr. Ali Farzi and the university of Tabriz, for his valuable guidance, scientific support, and financial support through the research grant that facilitated the development and construction of the experimental setup used in this study.

References

[1] L. Bing *et al.*, "Global and National CO 2 Emission from Lime Production Process and Carbonation sink from 1930 to 2024," *Earth Syst. Sci. Data Discuss.*, vol. 2026, pp. 1–27, 2026.

[2] M. Hussaini *et al.*, "Assessing the Atmospheric Concentrations of Carbon Monoxide (CO) and Carbon Dioxide (CO_2) in the Urban Environment in Maiduguri Metropolis," *African J. Environ. Sci. Renew. Energy*, vol. 22, no. 1, pp. 52–70, 2026.

[3] I. C. Change, "The physical science basis," *(No Title)*, 2013.

[4] F. Raganati and P. Ammendola, "CO2 post-combustion capture: a critical review of current technologies and future directions," *Energy & Fuels*, vol. 38, no. 15, pp. 13858–13905, 2024.

[5] K. Zhang and R. Wang, "A critical review on new and efficient adsorbents for CO2 capture," *Chem. Eng. J.*, vol. 485, p. 149495, 2024.

[6] A. Das *et al.*, "Advancements in adsorption based carbon dioxide capture technologies-A comprehensive review," *Heliyon*, vol. 9, no. 12, 2023.

[7] P. D. Dissanayake *et al.*, "Biochar-based adsorbents for carbon dioxide capture: A critical review," *Renew. Sustain. Energy Rev.*, vol. 119, p. 109582, 2020.

[8] X. Xu, Y. Zhao, J. Sima, L. Zhao, O. Mašek, and X. Cao, "Indispensable role of biochar-inherent mineral constituents in its environmental applications: A review," *Bioresour. Technol.*, vol. 241, pp. 887–899, 2017.

[9] C. Zhang *et al.*, "The application of biochar for CO2 capture: influence of biochar preparation and CO2 capture reactors," *Ind. Eng. Chem. Res.*, vol. 62, no. 42, pp. 17168–17181, 2023.

[10] W. Tian *et al.*, "Amine-modified biochar for the efficient adsorption of carbon dioxide in flue gas," *Atmosphere (Basel).*, vol. 13, no. 4, p. 579, 2022.

[11] L. Fang *et al.*, "Biochar-based materials in environmental pollutant elimination, H2

production and CO2 capture applications," *Biochar*, vol. 5, no. 1, p. 42, 2023.

[12] E. A. P. Dias, D. G. da Silva, M. da Costa Amaral, L. dos Santos Pereira, D. C. de Melo, and W. L. Vasconcelos, "CO2 adsorption by zeolites: State-of-Art, techniques and emerging trends," *Microporous Mesoporous Mater.*, p. 113904, 2025.

[13] D. G. Boer, J. Langerak, and P. P. Pescarmona, "Zeolites as selective adsorbents for CO2 separation," *ACS Appl. Energy Mater.*, vol. 6, no. 5, pp. 2634–2656, 2023.

[14] L. Bénariac-Doumal *et al.*, "A comparative study of CO 2 adsorption in a series of zeolites," *Phys. Chem. Chem. Phys.*, vol. 27, no. 20, pp. 10621–10634, 2025.

[15] V. Garshasbi, M. Jahangiri, and M. Anbia, "Equilibrium CO2 adsorption on zeolite 13X prepared from natural clays," *Appl. Surf. Sci.*, vol. 393, pp. 225–233, 2017.

[16] Y. Li, R. Gupta, Q. Zhang, and S. You, "Review of biochar production via crop residue pyrolysis: Development and perspectives," *Bioresour. Technol.*, vol. 369, p. 128423, 2023.

[17] A. Tomczyk, Z. Sokołowska, and P. Boguta, "Biochar physicochemical properties: pyrolysis temperature and feedstock kind effects," *Rev. Environ. Sci. Bio/Technology*, vol. 19, no. 1, pp. 191–215, 2020.

[18] E. Cárdenas-Aguiar, A. Méndez, G. Gascó, M. Lado, and A. Paz-González, "The effects of feedstock, pyrolysis temperature, and residence time on the properties and uses of biochar from broom and gorse wastes," *Appl. Sci.*, vol. 14, no. 10, p. 4283, 2024.

[19] D. Liang *et al.*, "Construction of biochar-zeolite composite for enhanced VOCs adsorption: Interfacial reinforcement and steam-driven synergistic regulation of pore formation and dealumination," *J. Clean. Prod.*, vol. 524, p. 146481, 2025.

[20] V. P. Mulgundmath, R. A. Jones, F. H. Tezel, and J. Thibault, "Fixed bed adsorption for the removal of carbon dioxide from nitrogen: breakthrough behaviour and modelling for heat and mass transfer," *Sep. Purif. Technol.*, vol. 85, pp. 17–27, 2012.

[21] P. A. Saenz Cavazos, E. Hunter-Sellars, P. Iacomi, S. R. McIntyre, D. Danaci, and D. R. Williams, "Evaluating solid sorbents for CO2 capture: linking material properties and process efficiency via adsorption performance," *Front. Energy Res.*, vol. 11, p. 1167043, 2023.

[22] W. Cao *et al.*, "Novel post-treatment of ultrasound assisting with acid washing enhance lignin-based biochar for CO2 capture: adsorption performance and mechanism," *Chem. Eng. J.*, vol. 471, p. 144523, 2023.

[23] Y. Liu *et al.*, "Activation and functionalization of biochar-based catalysts obtained from sewage sludge and cotton stalks to improve hydrogen-rich gas production," *J. Environ. Chem. Eng.*, vol. 13, no. 5, p. 117665, 2025.

[24] Y. Zhang *et al.*, "Relationship of CO2 adsorption performance and physicochemical property of biochar prepared by different types of biomass waste," *J. Environ. Chem. Eng.*, vol. 12, no. 6, p. 114571, 2024.

[25] C. Chen, D.-W. Park, and W.-S. Ahn, "CO2 capture using zeolite 13X prepared from bentonite," *Appl. Surf. Sci.*, vol. 292, pp. 63–67, 2014.

[26] L. Wang *et al.*, "Enhancing the CO2 adsorption performance on 13× zeolite by

optimising K+ ion-exchange degree," *Chem. Eng. J.*, p. 169893, 2025.

[27] A. Faggiano *et al.*, "Optimizing CO2 capture: Effects of chemical functionalization on woodchip biochar adsorption performance," *J. Environ. Manage.*, vol. 380, p. 125059, 2025.

[28] K. B. Jivrakh *et al.*, "3D-printed zeolite 13X gyroid monolith adsorbents for CO2 capture," *Chem. Eng. J.*, vol. 497, p. 154674, 2024.

[29] M. Aghaei, M. Anbia, and S. Salehi, "Measurements and modeling of CO2 adsorption behaviors on granular zeolite 13X: Impact of temperature and time of calcination on granules properties in granulation process using organic binders," *Environ. Prog. Sustain. Energy*, vol. 41, no. 5, p. e13866, 2022.

[30] K. Yang, J. Wu, C. Li, Y. Xiang, and G. Yang, "Efficient method to obtain the force field for CO2 adsorption on zeolite 13X: understanding the host–guest interaction mechanisms of low-pressure adsorption," *J. Phys. Chem. C*, vol. 124, no. 1, pp. 544–556, 2019.

[31] E. Khoramzadeh, M. Mofarahi, K. Chung, and C.-H. Lee, "Equilibrium adsorption and kinetic study of CO2 and N2 on synthesized carbon Black–Zeolite composite," *Sep. Purif. Technol.*, vol. 280, p. 119917, 2022.

[32] H. Jedli, S. M. Bouzgarrou, R. Hassani, E. Sabi, and K. Slimi, "CO2 Adsorption on Mesoporous Silica Using Response Surface Methodology (RSM)," *Asia-Pacific J. Chem. Eng.*, vol. 21, no. 1, p. e70141, 2026.

[33] M. Ahmadi, F. Bahmanzadegan, M. Qasemnazhand, A. Ghaemi, and H. Ramezanipour Penchah, "Experimental, RSM modelling, and DFT simulation of CO2 adsorption on Modified activated carbon with LiOH," *Sci. Rep.*, vol. 14, no. 1, p. 13595, 2024.

[34] M. Xu *et al.*, "Optimizing adsorption of 17α-ethinylestradiol from water by magnetic mxene using response surface methodology and adsorption kinetics, isotherm, and thermodynamics studies," *Molecules*, vol. 26, no. 11, p. 3150, 2021.

[35] S. Tibebu, A. Worku, T. G. Weldmichael, and M. Aschale, "Optimization of biochar production from Rumex abyssinicus using response surface methodology and its application in amending degraded soil," *Sci. Rep.*, 2025.

[36] F. Fathalian, H. Moghadamzadeh, A. Hemmati, and A. Ghaemi, "Efficient CO2 adsorption using chitosan, graphene oxide, and zinc oxide composite," *Sci. Rep.*, vol. 14, no. 1, p. 3186, 2024.

[37] P. Borisut, C. Tangsathitkulchai, and A. Nuchitprasittichai, "Dynamic of CO2 adsorption in a fixed bed of microporous and mesoporous activated carbon impregnated with sodium hydroxide and the application of response surface methodology (RSM) for determining optimal adsorption conditions," *Environ. Sci. Pollut. Res.*, vol. 31, no. 9, pp. 13833–13855, 2024.

[38] F. Bahmanzadegan, M. A. Pordsari, and A. Ghaemi, "Improving the efficiency of 4A-zeolite synthesized from kaolin by amine functionalization for CO2 capture," *Sci. Rep.*, vol. 13, no. 1, p. 12533, 2023.

[39] S. W. A. Shah *et al.*, "Response surface methodology for optimization of operational parameters to remove ciprofloxacin from contaminated water in the presence of a bacterial consortium," *Acs Omega*, vol. 7, no. 31, pp. 27450–27457, 2022.

[40] M. C. Ndoun and S. A. Darko, “Characterization and Evaluation of Carbonaceous Materials from the Hydrothermal Carbonization of Waste Pharmaceuticals,” *arXiv Prepr. arXiv2302.06020*, 2023.

[41] S. K. R. Velagala, A. Pore, Y. Sabri, R. Parthasarathy, and I. Sreedhar, “Enhanced and Stable Carbon Capture through Hierarchical Sorbent and Process Optimization Using Biochar from Deoiled Cake,” *ACS Omega*, 2026.

[42] Z. Khoshraftar, A. Ghaemi, and A. Hemmati, “Comprehensive investigation of isotherm, RSM, and ANN modeling of CO2 capture by multi-walled carbon nanotube,” *Sci. Rep.*, vol. 14, no. 1, p. 5130, 2024.

[43] H. Jedli, M. Almonnef, R. Rabhi, M. Mbarek, J. Abdessalem, and K. Slimi, “Activated carbon as an adsorbent for CO2 capture: adsorption, kinetics, and RSM modeling,” *ACS omega*, vol. 9, no. 2, pp. 2080–2087, 2023.

[44] P. Arjona-Jaime, E. D. Isaacs-Paez, C. Nieto-Delgado, L. F. Chazaro-Ruiz, and R. Rangel-Mendez, “Insight into the effect of pressure on the CO2 capture capacity and kinetics by a biochar-ionic liquid composite,” *J. Environ. Chem. Eng.*, vol. 12, no. 1, p. 111804, 2024.

[45] E. Luzzi, P. Aprea, M. Salzano de Luna, D. Caputo, and G. Filippone, “Mechanically coherent zeolite 13X/chitosan aerogel beads for effective CO2 capture,” *ACS Appl. Mater. Interfaces*, vol. 13, no. 17, pp. 20728–20734, 2021.

[46] A. J. Ringsby, C. M. Ross, and K. Maher, “Sorption of soil carbon dioxide by biochar and engineered porous carbons,” *Environ. Sci. Technol.*, vol. 58, no. 19, pp. 8313–8325, 2024.

[47] S. Khalili, B. Khoshandam, and M. Jahanshahi, “Optimization of production conditions for synthesis of chemically activated carbon produced from pine cone using response surface methodology for CO2 adsorption,” *RSC Adv.*, vol. 5, no. 114, pp. 94115–94129, 2015.

[48] Y. Liu, H. Fang, S. Zhang, C. Wang, and L. Min, “Enhanced CO2 Adsorption of Alkali-Modified Sludge Biochar via Hydrothermal Activation: Mechanisms and Kinetics,” *Case Stud. Constr. Mater.*, p. e05250, 2025.

[49] S. Lagergren, “Zur theorie der sogenannten adsorption geloster stoffe,” 1898.

[50] Y.-S. Ho and G. McKay, “Pseudo-second order model for sorption processes,” *Process Biochem.*, vol. 34, no. 5, pp. 451–465, 1999.

[51] A. H. Whaieb *et al.*, “A comprehensive study of CO2 capture using attapulgite and novel hybrid Attapulgite/13X zeolite composite: kinetic, isotherm, and thermodynamic analysis,” *Microporous Mesoporous Mater.*, p. 113770, 2025.

[52] J.-S. Lee, J.-H. Kim, J.-T. Kim, J.-K. Suh, J.-M. Lee, and C.-H. Lee, “Adsorption equilibria of CO2 on zeolite 13X and zeolite X/activated carbon composite,” *J. Chem. Eng. Data*, vol. 47, no. 5, pp. 1237–1242, 2002.

[53] A. I. Sarker, A. Aroonwilas, and A. Veawab, “Equilibrium and kinetic behaviour of CO2 adsorption onto zeolites, carbon molecular sieve and activated carbons,” *Energy Procedia*, vol. 114, pp. 2450–2459, 2017.

[54] R. Chatterjee *et al.*, “Effect of pyrolysis temperature on physicochemical properties and

acoustic-based amination of biochar for efficient CO2 adsorption," *Front. Energy Res.*, vol. 8, p. 85, 2020.

[55] A. Wahby *et al.*, "Recent advances in biochar-based engineered materials for efficient removal of CO2: from lab to industrial scale applications," *Environ. Sci. Adv.*, vol. 5, no. 4, pp. 997–1026, 2026.

[56] Y. Yin *et al.*, "Synthesis of zeolite molecular sieve 13X from coal-fired slag for efficient room temperature CO2 adsorption," *Chem. Eng. Sci.*, vol. 288, p. 119838, 2024.

[57] S. Karka, S. Kodukula, S. V Nandury, and U. Pal, "Polyethylenimine-modified zeolite 13X for CO2 capture: adsorption and kinetic studies," *ACS omega*, vol. 4, no. 15, pp. 16441–16449, 2019.

[58] C. Zhang, S. Sun, S. He, and C. Wu, "Direct air capture of CO2 by KOH-activated bamboo biochar," *J. Energy Inst.*, vol. 105, pp. 399–405, 2022.

[59] S. Kuloglija *et al.*, "Isotherms and kinetics of CO_2 adsorption on biochar-based activated carbon for sustainable climate solutions," *Sep. Purif. Technol.*, p. 136079, 2025.

[60] X. Yuan, J. Xiao, M. Yılmaz, T. C. Zhang, and S. Yuan, "N, P Co-doped porous biochar derived from cornstalk for high performance CO2 adsorption and electrochemical energy storage," *Sep. Purif. Technol.*, vol. 299, p. 121719, 2022.

[61] S. Guo, Y. Li, Y. Wang, L. Wang, Y. Sun, and L. Liu, "Recent advances in biochar-based adsorbents for CO2 capture," *Carbon Capture Sci. Technol.*, vol. 4, p. 100059, 2022.

[62] B. Feizi-Afshar, L. Vafajoo, and A. Farzi, "A decade of advances in agricultural waste-derived biochar for direct air CO2 capture: Activation, modification, and performance trends," *Results Chem.*, p. 102921, 2025.